Mean Inner Potential of Liquid Water

Murat Nulati Yesibolati, Simone Laganà, Hongyu Sun, Marco Beleggia, Shawn M. Kathmann, Takeshi Kasama, and Kristian Mølhave

Phys. Rev. Lett. **124**, 065502 — Published 13 February 2020

DOI: 10.1103/PhysRevLett.124.065502

The Mean Inner Potential of Liquid Water

Murat Nulati Yesibolati[1], Simone Laganà[1], Hongyu Sun[1], Marco Beleggia[1], Shawn M. Kathmann[2,*], Takeshi Kasama[1,†], Kristian Mølhave[1,*]

[1]DTU Nanolab, National Centre for Nano Fabrication and Characterization, Technical University of Denmark, Building 307, 2800 Kgs. Lyngby, Denmark

[2]Physical Sciences Division, Pacific Northwest National Laboratory, 902 Battelle Boulevard, P.O. Box 999, Richland WA 99352, USA.

*Correspondence to: E-mail: krmo@dtu.dk (K.M.); Shawn.Kathmann@pnnl.gov (S.M.K.).

[†]In memory of Takeshi Kasama, deceased 22.05.2019

Abstract:
Improving our experimental and theoretical knowledge of electric potentials at liquid-solid boundaries is essential to achieve a deeper understanding of the driving forces behind interfacial processes. Electron holography has proved successful in probing solid-solid interfaces but requires knowledge of the materials' mean inner potential (MIP, V_0), which is a fundamental bulk material property. Combining off-axis electron holography with liquid phase transmission electron microscopy (LPTEM), we provide the first quantitative MIP determination of liquid water V_0=+4.48±0.19 V. This value is larger than most theoretical predictions, and to explain the disagreement we assess the dominant factors needed in quantum simulations of liquid water. A precise MIP lays the foundations for nanoscale holographic potential measurements in liquids, and provides a benchmark to improve quantum mechanical descriptions of aqueous systems and their interfaces in e.g. electrochemistry, solvation processes and spectroscopy.

Introduction: The mean inner potential (MIP, V_0) is the volume-averaged electrostatic potential of a material with respect to a distant vacuum reference region at zero volts. The MIP is an intrinsic material property that depends on its elemental composition, structure, and electronic configuration [1]. The MIP is also known as the Bethe potential since Hans Bethe was the first to derive it [2], and provides an essential benchmark for both classical [3] and quantum mechanical (QM) molecular modeling [4], especially when studying electrodynamics of materials. For liquid water in particular, acquiring a reliable experimental MIP will benefit the accurate quantification of a variety of processes, e.g., for theoretical prediction and data interpretation of photoelectron spectroscopy (PES) [5,6], and will shed light on the nature of surface potentials, which is a source of debate in various scientific communities [7]. Using the MIP as a benchmark will also lead to improvements in models of aqueous systems where electrical potentials/fields at interfaces influence ion solvation processes [3], Stark vibrational spectroscopy [8], and electrocatalysis [9], where QM models preferably should be able to predict a reliable MIP before being used. Hence, rigorous MIP measurements and theoretical representations are essential to improve our understanding of water's electric properties and thereby our capabilities to predict and rationally design processes involving aqueous systems.

The MIP can also be characterized as an electric potential jump [3] experienced by an electron when crossing the surface from vacuum to the bulk material. It can be influenced by the material's surface termination, that in the past may have caused some discrepancies [10]. For a well-defined surface and bulk structure, the MIP is indeed experimentally and QM well-defined.

In the simplest quantum approximation, called the Independent Atom Model (IAM), isolated atoms in vacuum are superimposed at the relevant density to estimate an upper bound of the MIP (V_0) using Dirac-Fock electron scattering factors $f_i^e(0)$ at zero angle for the i atoms in a unit cell of volume Ω [11-13]

$$V_0^{\mathrm{IAM}} = \frac{(h^2/2\pi m_e e)}{\Omega} \sum f_i^e(0). \quad (1)$$

For liquid water at 25 °C, $V_0^{\mathrm{water,\,IAM}} = +4.87\mathrm{V}$ [3,14,15]. Current X-ray and electron diffraction measurements rely on the IAM to obtain atomic electron densities and potentials, respectively [4,15,16], however, a more accurate MIP would be a significant improvement.

In QM density functional theory (DFT), the MIP can be calculated by either averaging the total electric potential from an all-electron simulation, or by summing the contribution of the surface dipole layer and bulk quadrupole contributions [12,17] using Maximally Localized Wannier centers [18]. Table 1 summarizes published experimental and theoretical water MIP values, and also density corrected values [3,4,18-22], as the MIP is proportional to mass density via the unit cell volume Ω [23,24]. The quantum MIP values for vitreous ice and water vary significantly around +3.72 V (as corrected via the liquid density), the only previously reported experimental MIP value based on vitrified ice [21]. Some DFT models employ nuclear core corrections [4,19], where the true nuclear Z/r potential, from the nuclear delta function of charge Z, is used in the actual MIP calculation, rather than the very narrow Gaussian nuclei used for numerical purposes. Thus, an accurate measurement of the MIP of liquid water provides an essential guiding benchmark for improving quantum descriptions of water.

Table 1. Theoretical and Experimental MIP values

V_0 [V]	Method	V_0 [V] @ 1g/cm^3

<4.87	IAM	<4.49
3.63	DFT[18]	3.94
3.1 ± 0.2	DFT [3]	3.87
3.8 ± 0.2	DFT [4]	3.8
~3.70	DFT [20]	~3.4
4.32	DFT [19]	4.32
3.5±1.2	TEM [21]	3.72
3.5±0.5	TEM [22]	3.5

Off-axis electron holography in a transmission electron microscope (TEM) is one of the most accurate methods to measure the MIP as well as mapping out the electric potentials through materials and their interfaces [25]. However, liquids have not been measured reliably, due to evaporation in the TEM vacuum, charging and radiation damage [26,27], as well as a lack of accurate thickness measurements when using chip-based liquid phase TEM (LPTEM) [28]. To date, the only water MIP $V_0^{ice} = +3.5 \pm 1.2$ V [21] was measured on an amorphous vitrified ice sample at cryogenic temperature, by measuring the electron wave phase shift through polystyrene spheres with a known MIP relative to that of the surrounding vitrified ice. This value could include systematic errors from charging, thermal expansion [23,24] of both materials, and recrystallization. Recently, an estimated thickness of a single water droplet in LPTEM gave $V_0^{water} = +3.5 \pm 0.5$ V [22].

We present the first quantitative experimental liquid water MIP measurements by developing a novel LPTEM nanochannel liquid cell system [29] (Fig. 1a, and Supplemental Material S1 [30])and using electron holography to measure the phase change of the electron wave after passing through liquid water of known thickness (Supplemental Material S2 [30]). Assuming unbiased nonmagnetic materials, the electron wave phase shift ($\Delta\varphi$), relative to a reference wave passing through vacuum, is proportional to liquid thickness t and MIP, V_0 as [25]

$$\Delta\varphi = C_E V_0 \, t, \quad C_E = \frac{2\pi}{\lambda} \frac{E+E_0}{E(E+2E_0)}. \tag{2}$$

C_E is a constant that depends on the TEM beam energy (E). λ is the relativistic electron wavelength and E_0=511 keV is the rest mass energy of the electron. At 300 kV, C_E=6.53 × 10^6 rad/(Vm) [31]. The holographic interference image in Fig. 1b is of a nanochannel filled with liquid water and a stable radiolytic gas bubble. Holographic image reconstruction provides the phase image as in Fig. 1c.

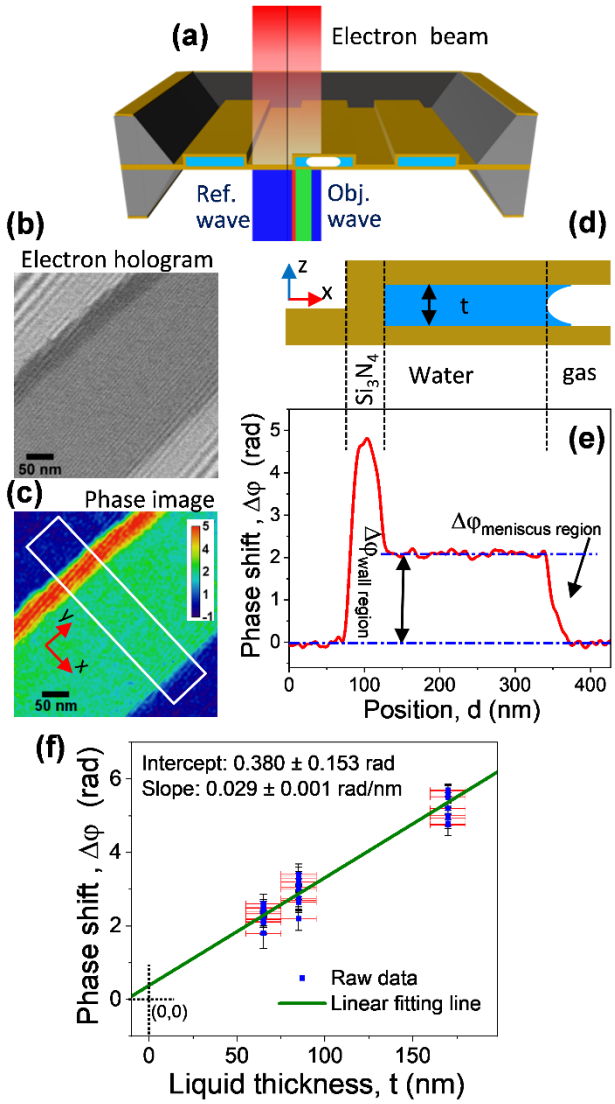

FIG. 1. **Thickness based MIP measurement.** **(a)** Illustration of the setup for nanochannel LPTEM off-axis electron holography. Interference of object and reference waves create the interference hologram in **(b)** of water near a nanochannel sidewall, with a stable meniscus to a bubble in the channel. **(c)** Reconstructed phase image with color code of Δφ in radian. **(d)** Schematic nanochannel cross-section with liquid thickness t. **(e)** Phase profile along the x-direction from white box in (c); Δφ was averaged over 80 nm in the y-direction. **(f)** Liquid water Δφ from three channels with liquid thickness t, and linear fit $\Delta\varphi = C_E V_0^{water,t} t + a$.

As shown in Fig. c and e, Si_3N_4 has larger MIP than water, therefore, the Si_3N_4 sidewall gives a larger phase shift. The water MIP is measured from the phase profile plateau relative to outside the channel, Fig. 1e. The holographic analysis, assumptions and QM simulations are further described in Supplemental Material S3-S4 [30]. Electron beam current and charging influence were found to be negligible, as detailed in Supplemental Materials S5 and S6 [30].

Three nanochannel liquid cells were used with different liquid layer thicknesses t, independently verified by chip cross-section images taken by scanning electron microscopy (Supplementary Material S7 [30]). The correlation between liquid thickness and phase change is shown in Fig. 1f with

each data point representing different regions of a given chip and a linear fit as Eqn. 1, $\Delta\varphi = C_E V_0^{water,t} t + a$, including uncertainty from both phase and thickness. A fitted parameter a=0.38±0.15 radian was included to account for minor local variations in charging and thickness, as well as possible deviations from linearity for very thin layers [32] . The a-parameter is close to zero within the overall error bars, and for a thickness based measurement MIP $V_0^{water,\,t} = +4.48 \pm 0.19$ V.

A second analysis was done, using on the inelastic mean free path of electrons (λ_{IMFP}), based on the correlation between the phase and amplitude variation [33] in the meniscus with varying water layer thickness. Interference fringe formation [25] is based on coherent electrons and the holographic image analysis removes any inelastic electron scattering contribution. The reconstructed amplitude image is equivalent to a zero loss energy filtered image [33,34] related to λ_{IMFP} as

$$\frac{t}{\lambda_{\mathrm{IMFP}}} = -2 \times \ln \frac{A_{\mathrm{obj}}}{A_{\mathrm{ref}}} \quad . \tag{3}$$

Combined with Eqn. 2, a MIP, V_0^{λ} can be found without knowing the sample thickness

$$\frac{\Delta\varphi}{-2C_E \ln \frac{A_{obj}}{A_{ref}}} = V_0^{\lambda} \lambda_{IMFP} \quad , \tag{4}$$

An example of the correlation between phase and amplitude in the meniscus is shown in Fig 2a-c and more in Supplementary Materials S8 [30], with a linear fit as expected from Eqn. 4 of the phase shift, $\Delta\varphi$, versus $-\ln(A_{obj}/A_{ref})$, where amplitude in the meniscus A_{obj}, is normalized relative to the bubble region without liquid A_{ref}. This relies on knowing the holographic λ_{IMFP} with high precision which is expected to be shorter than that determined by electron energy loss spectrometry (EELS) TEM [35-38], as EELS cannot resolve the small losses that reduce coherence in holography. Here λ_{IMFP} is based on the part of the channel with known liquid layer thickness using Eqn. 3 as detailed in Supplementary Materials S8 [30], giving a holographic λ_{IMFP} =164 ± 40 nm, as expected smaller than published EELS based water λ_{IMFP} [39].

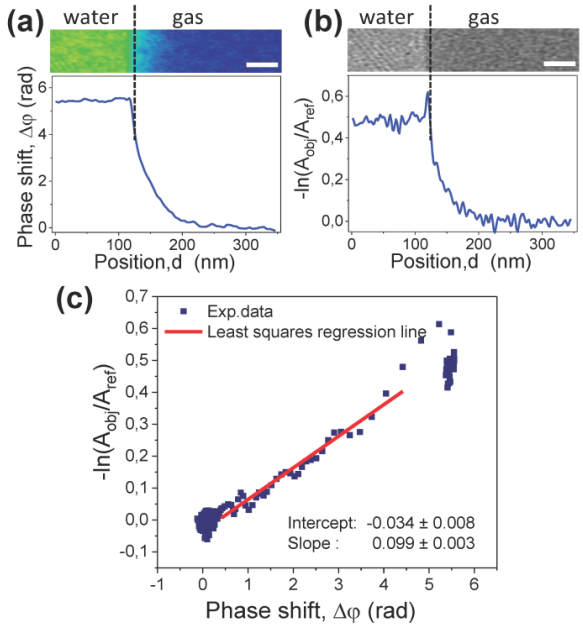

FIG. 2. **Example of λ_{IMFP} based water MIP measurement. (a)** phase image and corresponding profile plots near a meniscus; **(b)** the inverse logarithm of amplitude (A_{obj}) normalized to region without liquid (A_{ref}), and corresponding profile plots; **(c)** Plot of correlation and linear fit to $-\ln(A_{obj}/A_{ref})$ vs Δφ. The scale bar is 50 nm.

The linear fit as in Fig. 2c is only done in the thickness varying meniscus, and passes, within uncertainty, close to the origin, where the slight offset could be due to minor membrane thickness variations, or residual liquid/humid layers and vapor in the assumed empty bubble region, which is another reason for including the a-parameter in Fig. 1f. The λ_{IMFP} based MIP is $V_0^{water,\lambda} = +4.3 \pm 0.8$ V from averaging the slopes, agreeing well with the thickness based MIP (Fig. 2). With larger uncertainty and implicit λ_{IMFP} reliance on thickness, the λ_{IMFP} based MIP is considered a self-consistency check confirming $V_0^{water,t}$.

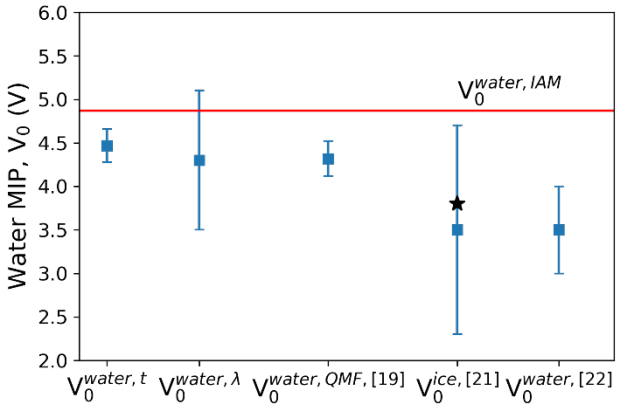

Fig 3. Comparison of water MIP values. From the nanochannel thickness based method, $V_0^{water,t}$; λ_{IMFP} based method, $V_0^{water,\lambda}$; the QMF model, $V_0^{water,QMF}$[19]; Measurements on vitrified ice, V_0^{ice}[21], also scaled to liquid density(★); and the water droplet estimate, V_0^{water} [22]. Red-solid line is the upper limit $V_0^{water,IAM}$.

The liquid water MIP values are larger than both the earlier measurement of vitrified ice [21] and the droplet estimated value [22], but partly within their upper uncertainty range. The vitrified ice result increases slightly when density-scaled from 0.94 to 1 g/cm^3 [23], and could be influenced by the degree of vitrification [24].

We consider the QM simulations of flexible water molecules (QMF) by Remsing et al. [19]. The QMF give a bulk quadrupole contribution $V_0^{\mathrm{water,QMF,bulk}} = 3.84\,\mathrm{V}$, 0.08V higher than the rigid model [4], indicating a negligible effect from flexibility. The QMF surface dipole contribution is $V_0^{\mathrm{water,QMF,surf.}} = +0.48\,\mathrm{V}$, which when added to $V_0^{\mathrm{water,QMF,bulk}}$ gives $V_0^{\mathrm{water,QMF}} = +4.32 \pm 0.20\,\mathrm{V}$ as the best matching theoretical MIP from Table 1, in excellent agreement with our measurements. The main difference between the QMF and the others listed in Table 1 is a combination of using the correct density, nuclear core correction that adds ca. +0.4 V, and the surface dipole addition. Importantly, the quantum and experimental MIPs are only about -0.5 V below the IAM upper limit MIP. This means that the total electronic redistribution (making OH bonds, lone pairs, and hydrogen bonding) in going from the IAM model to liquid water molecules only amounts to a MIP decrease of -0.5 V. We note that our MIP value is also in excellent agreement with water's diamagnetic susceptibility (Supplemental Material S9 [30]).

As noted, a reliable water MIP is important when comparing condensed bulk phase QM PES calculations with measurement, where the measured spectra are with respect to a vacuum at zero volts, similar to the reference potential for the holographic MIP. Using the MIP, all of the computed electronic energy levels must be corrected to the vacuum reference level [6]. In particular, the MIP of +4.48 V makes a large contribution to computed PES by shifting the electronic band offsets by more than 45% of the threshold ionization energy (~9.9 eV). Currently QM values around +3.7 V are used [20] to predict photoelectron ionization thresholds [5,6]. Beyond PES, solvation processes [3], and field-induced processes such as Stark vibrational spectroscopy [8] and electrocatalysis [9] would likely benefit from reliable MIPs to benchmark condensed phase electric potentials before calculating the fields underlying such processes.

In summary, we presented the first quantitative MIP measurement of liquid water at $V_0^{\mathrm{water,\,t}} = +4.48 \pm 0.19$ V, by combining off-axis electron holography with a nanochannel liquid phase TEM system, giving direct proportionality between the transmitted electron wave phase shift and liquid thickness. A self-consistency check was made with a method based on the inelastic mean free path of electrons. Both methods' MIPs are in excellent agreement and within error bars of the best available condensed phase quantum mechanical simulation including the correct liquid density, surface dipole potential, and nuclear core corrections. The values are below the IAM limit and within the upper uncertainty of vitrified ice measurements [21]. These measurements provide critical benchmarks for quantum mechanical simulations of electric potentials inside water and at its interfaces to matter. This novel MIP technique is fundamental to future electron holographic microscopy of electric potentials in nanoscale liquid processes.

Acknowledgments: This paper the authors acknowledge core facilities support from DTU Nanolab and DTU Health, and engineering support from Per Thor Jonassen, Wilhelmus Huyzer and Adam Fuller. The authors acknowledge helpful discussions with Nestor J. Zaluzec, Dwayne Miller, Tim Duigan, Rick Remsing, Marcel Baer, Chris Mundy, Gregory Schenter, Mohammad Koleini and Mads Brandbyge. **Funding:** The research was supported by Technical University of Denmark and from the Danish Research Council for Technology and Production Case No. 12-126194. S.M.K. was supported by the U.S. Department of Energy, Office of Science, Office of Basic Energy Sciences, Division of

Chemical Sciences, Geosciences & Biosciences. PNNL is operated by Battelle Memorial Institute for the U.S. Department of Energy under Contract No. DE-AC05-76RL01830. This research used resources of the National Energy Research Scientific Computing Center, which is supported by the Office of Science of the U.S. Department of Energy under Contract No. DE-AC02-05CH11231.

Author contributions: K.M. and M.N.Y. proposed and directed the research with help from S.L., T.K., S.M.K., M. B., H.Y. S. Chips were fabricated by S.L., and M.N.Y. engineered the custom-made TEM holder; M.N.Y. and T.K. carried out experiments and data analysis; S.M.K. implemented simulation; M.B. helped in charge analysis; H.Y.S. helped in experiment both in chip preparation and TEM operation. M.N.Y., K.M. and S.M.K. wrote the manuscript; all authors contributed to the discussion of the experimental results and revision of the text.

Competing interests: We declare no interests.

Data and materials availability: All data needed to draw the research conclusion are presented in the paper and supplementary information.

Supplementary Material includes Materials and methods (S1-S4), electron beam and charge influences (S5-S6), sample thickness measurement (S7), electron mean free path measurement (S8), discussion in diamagnetic susceptibility (S9) and supplementary references.

References

[1] J. C. H. Spence, Acta. Crystallogr. A **49**, 231 (1993).
[2] H. Bethe, Ann. Phys. (Berlin) **87**, 55 (1928).
[3] S. M. Kathmann, I. F. W. Kuo, C. J. Mundy, and G. K. Schenter, J. Phys. Chem. B **115**, 4369 (2011).
[4] B. Sellner and S. M. Kathmann, J. Chem. Phys. **141**, 18C534 (2014).
[5] G. Olivieri, K. M. Parry, C. J. Powell, D. J. Tobias, and M. A. Brown, J. Chem. Phys. **144**, 154704 (2016).
[6] A. P. Gaiduk, M. Govoni, R. Seidel, J. H. Skone, B. Winter, and G. Galli, J. Am. Chem. Soc. **138**, 6912 (2016).
[7] T. S. Hofer and P. H. Hünenberger, J. Chem. Phys. **148**, 222814 (2018).
[8] S. M. Gruenbaum, C. J. Tainter, L. Shi, Y. Ni, and J. L. Skinner, J. Chem. Theory Comput. **9**, 3109 (2013).
[9] M. Liu *et al.*, Nature **537**, 382 (2016).
[10] R. S. Pennington, C. B. Boothroyd, and R. E. Dunin-Borkowski, Ultramicroscopy **159**, 34 (2015).
[11] J. M. Cowley, in *Diffraction Physics (Third Edition)*, edited by J. M. Cowley (North-Holland, Amsterdam, 1995), pp. 77.
[12] M. Gajdardziska-Josifovska and A. H. Carim, in *Introduction to Electron Holography*, edited by E. Völkl, L. F. Allard, and D. C. Joy (Springer US, Boston, MA, 1999), pp. 267.
[13] A. Sanchez and M. A. Ochando, J. Phys. C. Solid State **18**, 33 (1985).
[14] D. Rez, P. Rez, and I. Grant, Acta. Crystallogr. A **50**, 481 (1994).
[15] L. M. Peng, Micron **30**, 625 (1999).
[16] J. M. Sorenson, G. Hura, R. M. Glaeser, and T. Head-Gordon, J. Chem. Phys. **113**, 9149 (2000).
[17] P. Becker and P. Coppens, Acta. Crystallogr. A **46**, 254 (1990).

[18] K. Leung, J. Phys. Chem. Lett. **1**, 496 (2010).
[19] R. C. Remsing, M. D. Baer, G. K. Schenter, C. J. Mundy, and J. D. Weeks, J. Phys. Chem. Lett. **5**, 2767 (2014).
[20] T. A. Pham, C. Zhang, E. Schwegler, and G. Galli, Phys. Rev. B **89**, 060202 (2014).
[21] A. Harsher and H. Lichte, *Inelastic mean free path and mean inner potential of carbon foil and vitrified ice measured with electron holography* (Iop Publishing Ltd, Bristol, 1998), Electron Microscopy 1998, Vol 1: General Interest and Instrumentation.
[22] T. Prozorov, T. P. Almeida, A. Kovács, and R. E. Dunin-Borkowski, J. R. Soc. Interface **14** (2017).
[23] J. A. Ghormley and C. J. Hochanadel, Science **171**, 62 (1971).
[24] Y. Huang, X. Zhang, Z. Ma, W. Li, Y. Zhou, J. Zhou, W. Zheng, and C. Q. Sun, Sci. Rep. **3**, 3005 (2013).
[25] E. Völkl, L. F. Allard, and D. C. Joy, *Introduction to Electron Holography* (Kluwer Academic/Plenum Publishers, New York, 1999).
[26] M. Shirai, T. Tanigaki, S. Aizawa, H. S. Park, T. Matsuda, and D. Shindo, Ultramicroscopy **146**, 125 (2014).
[27] N. M. Schneider, M. M. Norton, B. J. Mendel, J. M. Grogan, F. M. Ross, and H. H. Bau, J. Phys. Chem. C **118**, 22373 (2014).
[28] F. M. Ross, Science **350** (2015).
[29] S. Lagana, E. K. Mikkelsen, H. Sun, R. Marie, and K. Mølhave, The 16th European Microscopy Congress 2016, Lyon France, , 5763 (2016).
[30] See Supplemental Material at [URL will be inserted by publisher] for Materials and methods (S1-S4), electron beam and charge influences (S5-S6), sample thickness measurement (S7), electron mean free path measurement (S8) and discussion of diamagnetic susceptibility (S9), which includes Refs. [40–53].
[31] T. Kasama, R. E. Dunin-Borkowski, and M. Beleggia, in *Electron Holography of Magnetic Materials*, edited by F. A. M. Ramirez (intechopen, intechopen, 2011).
[32] M. Wanner, D. Bach, D. Gerthsen, R. Werner, and B. Tesche, Ultramicroscopy **106**, 341 (2006).
[33] M. Gajdardziskajosifovska and M. R. Mccartney, Ultramicroscopy **53**, 291 (1994).
[34] M. R. McCartney and M. Gajdardziska-Josifovska, Ultramicroscopy **53**, 283 (1994).
[35] Z. Gan, M. DiNezza, Y.-H. Zhang, D. J. Smith, and M. R. McCartney, Microsc. Microanal. **21**, 1406 (2015).
[36] C. Cassidy, A. Dhar, and T. Shintake, Appl. Phys. Lett. **110**, 163503 (2017).
[37] F. Kern, D. Wolf, P. Pschera, and A. Lubk, Ultramicroscopy **171**, 26 (2016).
[38] A. Lubk, D. Wolf, and H. Lichte, Ultramicroscopy **110**, 438 (2010).
[39] M. Tanase, J. Winterstein, R. Sharma, V. Aksyuk, G. Holland, and J. A. Liddle, Microsc. Microanal. **21**, 1629 (2015).
[40] S. Laganá, E. K. Mikkelsen, R. Marie, O. Hansen, and K. Mølhave, Microelectron. Eng. **176**, 71 (2017).
[41] P. A. Midgley, Micron **32**, 167 (2001).
[42] D. K. Saldin and J. C. H. Spence, Ultramicroscopy **55**, 397 (1994).
[43] J. E. Hirsch, Ann. Phys. (Berlin) **526**, 63 (2014).
[44] M. Beleggia, L. C. Gontard, and R. E. Dunin-Borkowski, J. Phys. D: Appl. Phys. **49**, 294003 (2016).
[45] M. Beleggia, T. Kasama, R. E. Dunin-Borkowski, S. Hofmann, and G. Pozzi, Appl. Phys. Lett. **98**, 243101 (2011).
[46] C. Gatel, A. Lubk, G. Pozzi, E. Snoeck, and M. Hÿtch, Phys. Rev. Lett. **111**, 025501 (2013).

[47] S. Bhattacharyya, C. T. Koch, Uuml, and M. Hle, J. Ceram. Soc. Jpn. **114**, 1005 (2006).
[48] T. Malis, S. C. Cheng, and R. F. Egerton, J. Electron. Micr. Tech. **8**, 193 (1988).
[49] R. F. Egerton and S. C. Cheng, Ultramicroscopy **21**, 231 (1987).
[50] D. R. G. Mitchell, J. Microsc. **224**, 187 (2006).
[51] L. Rosenfeld, Naturwissenschaften **17**, 49 (1929).
[52] R. R. Lunt, S. Kena-Cohen, J. B. Benziger, and S. R. Forrest, Phys. Rev. Lett. **102** (2009).
[53] *Physical Constants of Organic Compounds,Magnetic Susceptibility of Inorganic Materials, Internet Version* (CRC Press, Taylor & Francis Group, 2019), 100 edn., CRC Handbook of Chemistry and Physics.